

Article

# Enhanced Coercivity of Low-Density Barium Hexaferrite Magnets from Paste-Injection Molding

Wannisa Thongsamrit<sup>1,2</sup>, Pongsakorn Jantaratana<sup>3</sup>, Thanida Charoensuk<sup>1</sup> and Chitnarong Sirisathitkul<sup>1,4,\*</sup>

<sup>1</sup> Thailand Center of Excellence in Physics, Ministry of Higher Education, Science, Research and Innovation, 328 Si Ayutthaya Road, Bangkok 10400, Thailand; 61605076@kmitl.ac.th (W.T.); cthanida@mail.wu.ac.th (T.C.)

<sup>2</sup> Center of Excellence in Smart Materials Research and Innovation, King Mongkut's Institute of Technology Ladkrabang, Chalongkrung Road, Ladkrabang, Bangkok 10520, Thailand

<sup>3</sup> Department of Physics, Faculty of Science, Kasetsart University, 50 Ngam Wong Wan Road, Chatuchak, Bangkok 10900, Thailand; fscipsj@ku.ac.th

<sup>4</sup> Division of Physics, School of Science, Walailak University, Nakhon Si Thammarat 80160, Thailand

\* Correspondence: schitnar@mail.wu.ac.th

**Abstract:** Ceramic–polymer paste-injection molding is demonstrated as a facile fabrication route for barium hexaferrite magnets. Interestingly, these low-density (1.90–2.35 g/cm<sup>3</sup>) magnets exhibit substantial coercivity of 3868–4002 Oe. When ceramic paste without polymeric additives is used, reduced coercivity and slightly increased magnetizations are obtained from a magnet with the density of 2.55 g/cm<sup>3</sup>. Their magnetizations are also higher than those obtained from compactions of sol–gel-derived powders. For compact magnets (3.46–3.77 g/cm<sup>3</sup>), the DI water addition results in a slightly higher magnetization but lower coercivity than dry-pressed magnets. Compactions into disk and bar magnets give rise to comparable magnetic properties. The morphological characterizations reveal smaller barium hexaferrite particles leading to larger coercivity, and the density and shape of magnets have a less pronounced effect.

**Keywords:** barium hexaferrite; paste-injection molding; sol–gel auto-combustion; compact magnet



**Citation:** Thongsamrit, W.; Jantaratana, P.; Charoensuk, T.; Sirisathitkul, C. Enhanced Coercivity of Low-Density Barium Hexaferrite Magnets from Paste-Injection Molding. *Magnetochemistry* **2022**, *8*, 46. <https://doi.org/10.3390/magnetochemistry8040046>

Academic Editor: Yujie Yang

Received: 16 March 2022

Accepted: 13 April 2022

Published: 15 April 2022

**Publisher's Note:** MDPI stays neutral with regard to jurisdictional claims in published maps and institutional affiliations.



**Copyright:** © 2022 by the authors. Licensee MDPI, Basel, Switzerland. This article is an open access article distributed under the terms and conditions of the Creative Commons Attribution (CC BY) license (<https://creativecommons.org/licenses/by/4.0/>).

## 1. Introduction

Barium hexaferrites (BaFe<sub>12</sub>O<sub>19</sub>) and strontium hexaferrites (SrFe<sub>12</sub>O<sub>19</sub>) have a substantial market share in permanent magnets, high-frequency (30–100 GHz) devices, and data-storage applications [1,2]. These M-type hexagonal ferrites are also currently investigated for new other applications including electromagnetic wave absorbers and micro-magnets [1,3]. Their standout characteristics are large crystalline anisotropy and high chemical stability. Despite having moderate saturation magnetization, hexagonal ferrites are low-cost alternatives to rare-earth magnets [2,4].

Nanostructured hexagonal ferrites from chemical co-precipitation, ball-milling, hydrothermal, and sol–gel syntheses have been actively investigated [1]. Besides their utility in the form of nanoparticles, there are interests in producing permanent magnets from nanostructured hexagonal ferrites. Examples are hard/soft magnetic and ferrite polymer composites [1,2]. The sol–gel technique can synthesize a large batch of ferrite nanoparticles for fabricating bulk magnets [5–8].

Sintered and polymer-bonded ferrite magnets are traditionally manufactured using powder compaction and injection molding. The effects of compaction pressure on the density and magnetic properties of BaFe<sub>12</sub>O<sub>19</sub> have been investigated [9–11]. However, the reliance on molds limits a variety of shapes and dimensions of magnets. Recent developments in stereolithography, laser sintering, binder jetting, fuse-filament fabrication, and extrusion freeforming enable three-dimensional printing of ceramic magnets with complex shapes and varying dimensions [12]. Wei et al. demonstrated that extrusion freeforming could be a prime candidate for large-scale additive manufacturing of BaFe<sub>12</sub>O<sub>19</sub>

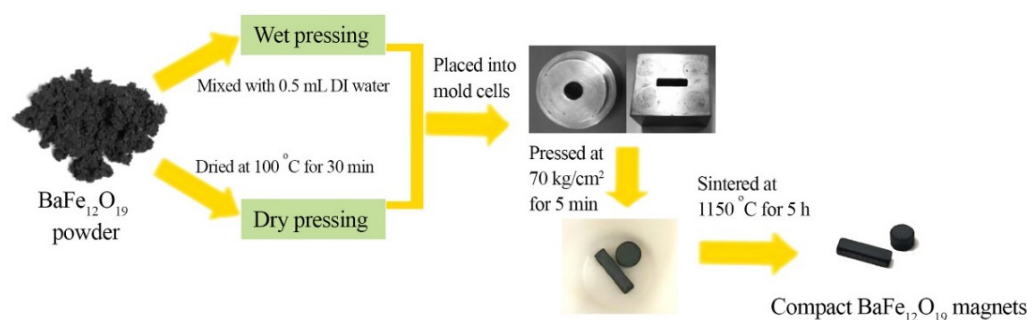
and  $\text{SrFe}_{12}\text{O}_{19}$  [13]. Using the same starting materials as traditional synthesis [14,15],  $\text{BaCO}_3$  and  $\text{Fe}_2\text{O}_3$  were mixed with water, organic binder, plasticizer, and dispersant. A large volume of ceramic paste could be facily printed or injected into molds.

This research deploys two routes to produce  $\text{BaFe}_{12}\text{O}_{19}$  magnets. The first method in Section 2.1 is the compaction of  $\text{BaFe}_{12}\text{O}_{19}$  powders derived by the sol-gel auto-combustion method. The other route is injection molding the aqueous ceramic paste, detailed in Section 2.2. After sintering the magnets from both methods at the same condition, their magnetic properties were compared and related to the phase, elemental compositions, morphology, and density.

## 2. Materials and Methods

### 2.1. $\text{BaFe}_{12}\text{O}_{19}$ Magnets from Powder Compaction

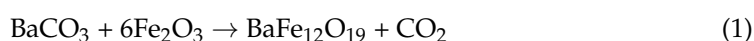
Following the procedure in [8], iron(III) nitrate nonahydrate ( $\text{Fe}(\text{NO}_3)_3 \cdot 9\text{H}_2\text{O}$ ) (more than 98.0% purity, Sigma-Aldrich, Singapore), and barium nitrate ( $\text{Ba}(\text{NO}_3)_2$ ) (more than 99.00% purity, Himedia, Andhra Pradesh, India) powders were used as precursors in sol-gel auto-combustion synthesis, followed by calcination at  $1050^\circ\text{C}$  for 3 h. The obtained  $\text{BaFe}_{12}\text{O}_{19}$  powders were thoroughly ground in a mortar and then sieved using a 100-mesh aperture before weighing. The compaction was split into a dry pressing and a wet pressing, as depicted in Figure 1. Powders for the dry pressing were heated at  $100^\circ\text{C}$  for 30 min and 2 g of each sample was placed into a stainless mold cell for disk ( $10\text{ mm}$  in diameter,  $6\text{ mm}$  thick) or bar ( $5 \times 5 \times 20\text{ mm}^3$ ) magnets. For the wet pressing,  $0.5\text{ mL}$  of deionized (DI) water was added before being placed into the mold cell.  $\text{BaFe}_{12}\text{O}_{19}$  magnets were pressed under the pressure of  $70\text{ kg/cm}^2$  for 5 min with an automatic hydraulic machine and subsequently sintered at  $1150^\circ\text{C}$  for 5 h.



**Figure 1.** Production steps for  $\text{BaFe}_{12}\text{O}_{19}$  magnets by powder compaction.

### 2.2. $\text{BaFe}_{12}\text{O}_{19}$ Magnets from Paste-Injection Molding

To prepare ceramic-polymer paste, 7 g of  $\text{BaCO}_3$  (more than 99.0% purity, HiMedia, Andhra Pradesh, India) and  $\text{Fe}_2\text{O}_3$  (99.0% purity, Sigma-Aldrich, Beijing, China) powders were mixed in a stoichiometric ratio of 1:6 and ground with a mortar before being sieved through a 100-mesh. Four samples (2CP1-2CP4) were prepared, firstly by mixing the  $\text{BaCO}_3/\text{Fe}_2\text{O}_3$  powders with the binder poly(vinyl alcohol) powder (PVA) ( $\sim 287\text{ mg}$ ). The plasticizer poly(ethylene glycol) (PEG-400) ( $\sim 150\text{ mg}$ ), the dispersing agent EFKA<sup>®</sup> FA4620 ( $\sim 20\text{ mg}$ ), and DI water ( $2.3\text{ mL}$ ) were then added. For sample 2CP5, the sequence of chemicals was added differently. The polymeric additives were firstly dissolved in  $2.3\text{ mL}$  DI water. The mixed  $\text{BaCO}_3/\text{Fe}_2\text{O}_3$  powders were added to the aqueous solution afterward. This order of mixing, as depicted in Figure 2, followed those published in [13]. The last sample (2C0) was prepared by only mixing the  $\text{BaCO}_3/\text{Fe}_2\text{O}_3$  powder with  $1.5\text{ mL}$  DI water to compare the density and magnetic properties in the absence of polymeric additives. Each homogeneous aqueous-based paste was injected into the mold using syringes and allowed to dry for 3 h at room temperature. Dried samples were sintered at  $1150^\circ\text{C}$  for 5 h and  $\text{BaFe}_{12}\text{O}_{19}$  magnets were obtained according to the following reaction [14,15].



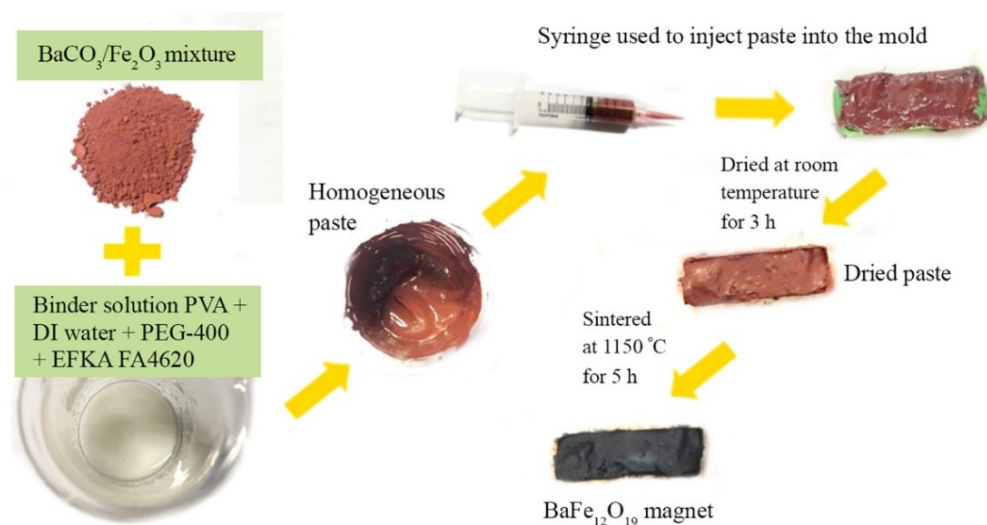


**Figure 2.** Production steps for  $\text{BaFe}_{12}\text{O}_{19}$  magnets from paste-injection molding (2CP5).

### 2.3. Characterizations of $\text{BaFe}_{12}\text{O}_{19}$ Magnets

The crystallographic phase was characterized by an X-ray diffractometer (XRD; Rigaku, SmartLab, Austin, TX, USA) using  $\text{CuK}\alpha 1$  radiation of  $1.54060 \text{ \AA}$ , in a  $2\theta$  range of  $20\text{--}80$  degrees. Morphology and elemental compositions were obtained by scanning electron microscopy (SEM; FEI, Quanta 250, Hillsboro, OR, USA) and energy-dispersive X-ray spectroscopy (EDS; Oxford, X-max50, Oxford, UK), respectively.

The density of each magnet was calculated from the ratio of mass (in g) to volume (in  $\text{cm}^3$ ). Magnetic properties were obtained by vibrating sample magnetometry (VSM; in-house developed and calibrated with Lakeshore 730908). VSM hysteresis loops traced the magnetization ( $M$ ) as a function of the external magnetic field ( $H$ ) between  $-17.5$  kOe and  $17.5$  kOe. The magnetic field was applied parallel to the horizontal plane of the bar and disk magnets. The remanent magnetization ( $M_r$ ) and the coercivity ( $H_c$ ) were determined from the  $y$ -intercept and the  $x$ -intercept, respectively.

## 3. Results and Discussion

All magnets in this study were sintered at  $1150 \text{ }^\circ\text{C}$  for 5 h. This condition follows previous reports [14,16] that the heat treatments at  $1050\text{--}1200 \text{ }^\circ\text{C}$  promote the pure  $\text{BaFe}_{12}\text{O}_{19}$  phase. XRD spectra in Figure 3 confirm the single  $\text{BaFe}_{12}\text{O}_{19}$  phase in both pressed magnets and paste-injection magnets. The characteristic peaks of the M-type  $\text{BaFe}_{12}\text{O}_{19}$  at  $30.38^\circ$ ,  $32.12^\circ$ ,  $34.22^\circ$ ,  $37.14^\circ$ ,  $40.44^\circ$ ,  $42.76^\circ$ ,  $55.14^\circ$ ,  $56.66^\circ$ ,  $63.24^\circ$ ,  $67.48^\circ$ , and  $72.64^\circ$  correspond to the crystallographic planes of (110), (107), (114), (203), (205), (206), (217), (2011), (220), (2014), and (1116), respectively (JCPDS: 01-74-1121). The difference from different processing routes is the intensity of the major diffraction peak at  $42.76^\circ$ . The sharp peaks in the case of compact magnets correspond to a smaller crystallite size obtained from the sol-gel synthesis.

SEM images in Figure 4 revealed the morphology of dry- and wet-pressed bar magnet and magnets from paste-injection molding. Particles are predominantly in the forms of hexagonal plate and short prism. The compact magnets (Figure 4a,b) have a wide cross-section distribution from  $550 \text{ nm}$  to  $2.5 \text{ }\mu\text{m}$ . The ceramic-polymer paste magnets (Figure 4c,d) generally contain particles of smaller sizes,  $350\text{--}950 \text{ nm}$ , consistent with the XRD peak broadening in Figure 3. However, some particles tend to agglomerate. Without polymer additives, particles in the ceramic paste magnet (Figure 4e) are notably larger. Their size distributions, ranging from  $850 \text{ nm}$  to  $2.2 \text{ }\mu\text{m}$ , are somewhat narrower than those of the compact magnets.

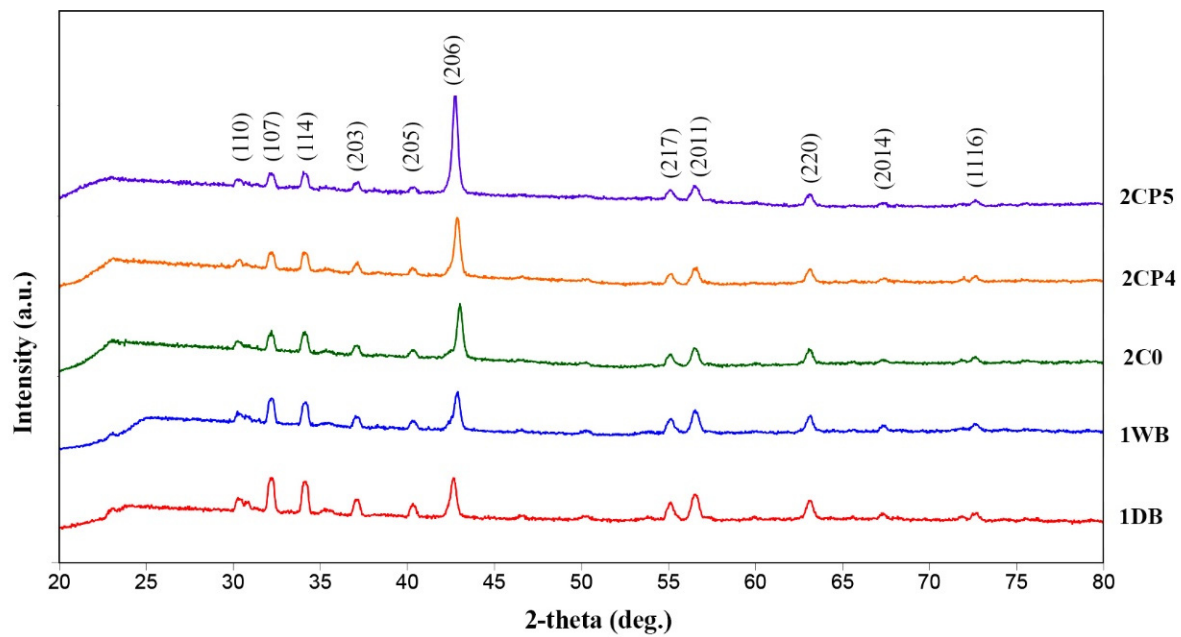
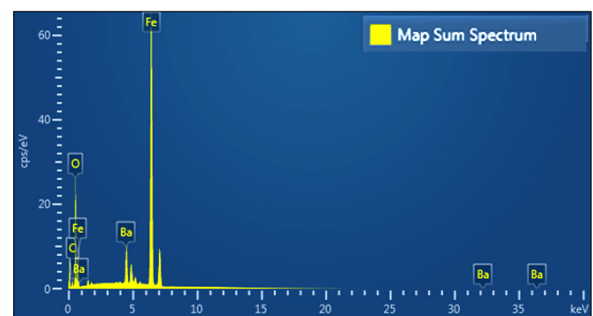
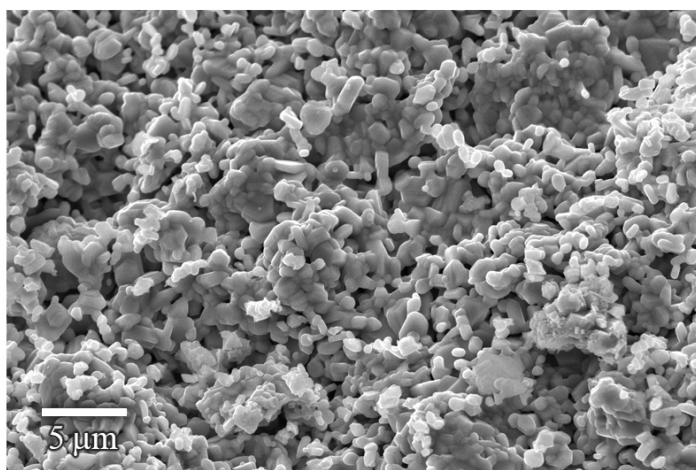
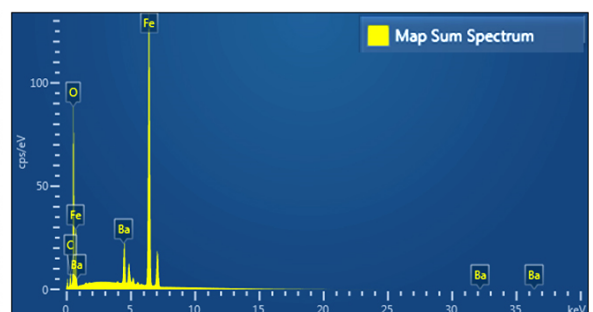
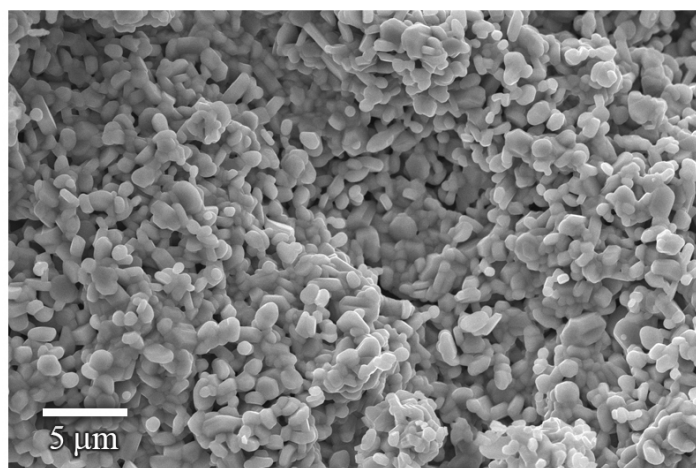


**Figure 3.** XRD spectra of the dry- and wet-pressed bar magnets (1DB and 1WB), and magnets from paste-injection molding (2C0, 2CP4 and 2CP5).



1DB magnet	Ba	Fe	O	C
Atomic percent	3.20	39.89	43.30	13.61
Atomic percent (no C)	3.70	46.17	50.12	—
Atomic ratio	1.00	12.47	13.53	—

(a)



1WB magnet	Ba	Fe	O	C
Atomic percent	2.41	27.80	50.93	18.86
Atomic percent (no C)	2.97	34.26	62.77	—
Atomic ratio	1.00	11.54	21.13	—

(b)

**Figure 4.** Cont.

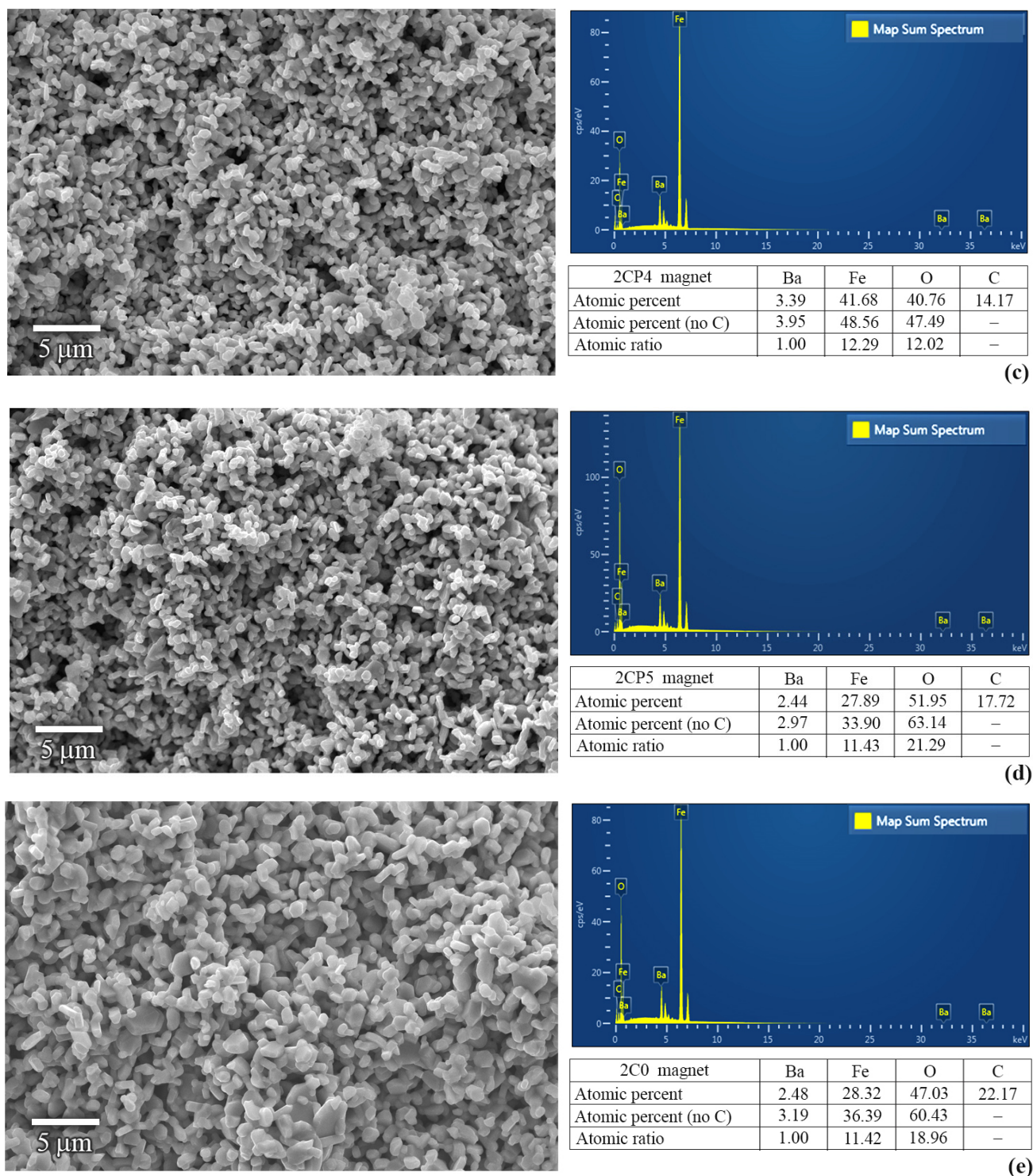


**Figure 4.** Morphology and elemental compositions of dry- and wet-pressed bar magnets, (a) 1DB; (b) 1WB; and magnets from paste-injection molding, (c) 2CP4; (d) 2CP5; (e) 2C0.

The EDS spectra, also shown in Figure 4, give the elemental composition mapping on the surface. The Fe, Ba, and O peaks are consistent with the phase identified by the XRD spectra. By subtracting the amount of C from the residual peak, the atomic percentages of Fe, Ba and O, were calculated. The Ba:Fe:O ratio of 1.00:11.42:18.96, closest to the stoichiometric ratio of  $\text{BaFe}_{12}\text{O}_{19}$ , was obtained in the 2C0 sample (Figure 4e). From the paste without polymer additives, the 2CP5 sample (Figure 4d) had a higher O composition

with a Ba:Fe:O ratio of 1.00:11.43:21.29. Such a difference will explain the different magnetic properties in the following discussion.

According to Table 1, the dry compaction has better control over the magnet density (3.60–3.63 g/cm<sup>3</sup>) than the wet-pressed magnets (3.46–3.77 g/cm<sup>3</sup>). All hysteresis loops in Figure 5 are smooth, consistent with the single BaFe<sub>12</sub>O<sub>19</sub> phase. A kink may be observed if other phases such as iron oxides are present [17]. The magnetization (M in the y-axis), which increased with increasing application of magnetic field (H in the x-axis), was not saturated under the maximum 17.5 kOe field. The saturation magnetization (M<sub>s</sub> in Table 1) was estimated from the y-intercept of the plot between M and 1/H<sup>2</sup> in a regime close to the maximum applied field using the law of approach to saturation described in [8]. In addition to obtaining experimental M<sub>s</sub>, a higher applied magnetic field may reveal different values of coercivity by overcoming the remaining domain-wall-pinning mechanism. Hysteresis loops in Figure 5a,b indicate comparable magnetic parameters of dry-pressed and wet-pressed magnets for both shapes. The shape of compact magnets shows insignificant influence on coercivity and magnetizations in Table 1. The magnetizations are comparable but the coercivity is lower than the values reported in [5–7].

Without high-pressure compaction, magnets from paste-injection molding have much lower densities. The reproducibility of the process was firstly investigated by comparing replicate samples (2CP1–2CP4). The density varied in a small range from 1.88–1.92 g/cm<sup>3</sup>. Interestingly, the coercivities in Figure 5c are substantially higher than those of compact magnets. On the other hand, the M<sub>r</sub>/M<sub>s</sub> ratios in Table 1 are slightly larger in the case of magnets from paste-injection molding. The values close to 0.5 correspond to isotropic magnets. The highest coercivity was 4002 Oe in sample 2CP5, which changed the order of chemical mixing from samples 2CP1–2CP4. The largest remanent and saturation magnetization of 35.81 and 73.38 emu/g were obtained from the ceramic paste without polymeric additives (sample 2C0). This sample had the highest density of 2.55 g/cm<sup>3</sup> and the lowest coercivity of 3714 Oe among magnets from paste-injection molding.

Magnetizations of BaFe<sub>12</sub>O<sub>19</sub> magnets strongly are increased with the phase purity and density. The highest density of 3.77 g/cm<sup>3</sup> in this study, comparable to those in previous experiments [1–11], is still much lower than the theoretical value. Such low densities are consistent with pores among particles, which are not densely packed in Figure 4. Interestingly, large magnetizations were still obtained, as shown in Table 1, and should be attributed to the single-phase BaFe<sub>12</sub>O<sub>19</sub>. The slight variations in magnetizations in Table 1 can be related to the varied elemental composition exemplified by EDS spectra. The highest magnetization was obtained in the case of sample 2C0 with a uniform Ba:Fe:O ratio close to 1:12:19. The different fabrication methods had a larger effect on the coercivity. The coercivity was substantially enhanced by the reduction of particle size from the paste injection, whereas the larger sol–gel-derived particles give rise to coercivity of less than 2500 Oe. This particle size effect is more pronounced than those of density and shape of magnets.

**Table 1.** Density and magnetic properties of the BaFe<sub>12</sub>O<sub>19</sub> magnets from powder compaction and paste-injection molding.

Samples	Fabrication Method	Density (g/cm <sup>3</sup> )	Magnetic Properties			
			H <sub>c</sub> (Oe)	M <sub>r</sub> (emu/g)	M <sub>s</sub> (emu/g)	M <sub>r</sub> /M <sub>s</sub>
1DD	Dry-pressed disc	3.63	2454	33.48	69.94	0.48
1DB	Dry-pressed bar	3.60	2453	32.63	68.48	0.48
1WD	Wet-pressed disc	3.77	2389	33.97	70.01	0.48
1WB	Wet-pressed bar	3.46	2450	34.29	70.85	0.48
2CP1-4	Ceramic–polymer paste *	1.90 ± 0.02	3868 ± 42	35.24 ± 0.57	72.55 ± 2.13	0.49
2CP5	Ceramic–polymer paste	2.35	4002	35.80	72.59	0.49
2C0	Ceramic paste	2.55	3714	35.81	73.38	0.49

\* Averaged from 4 samples.

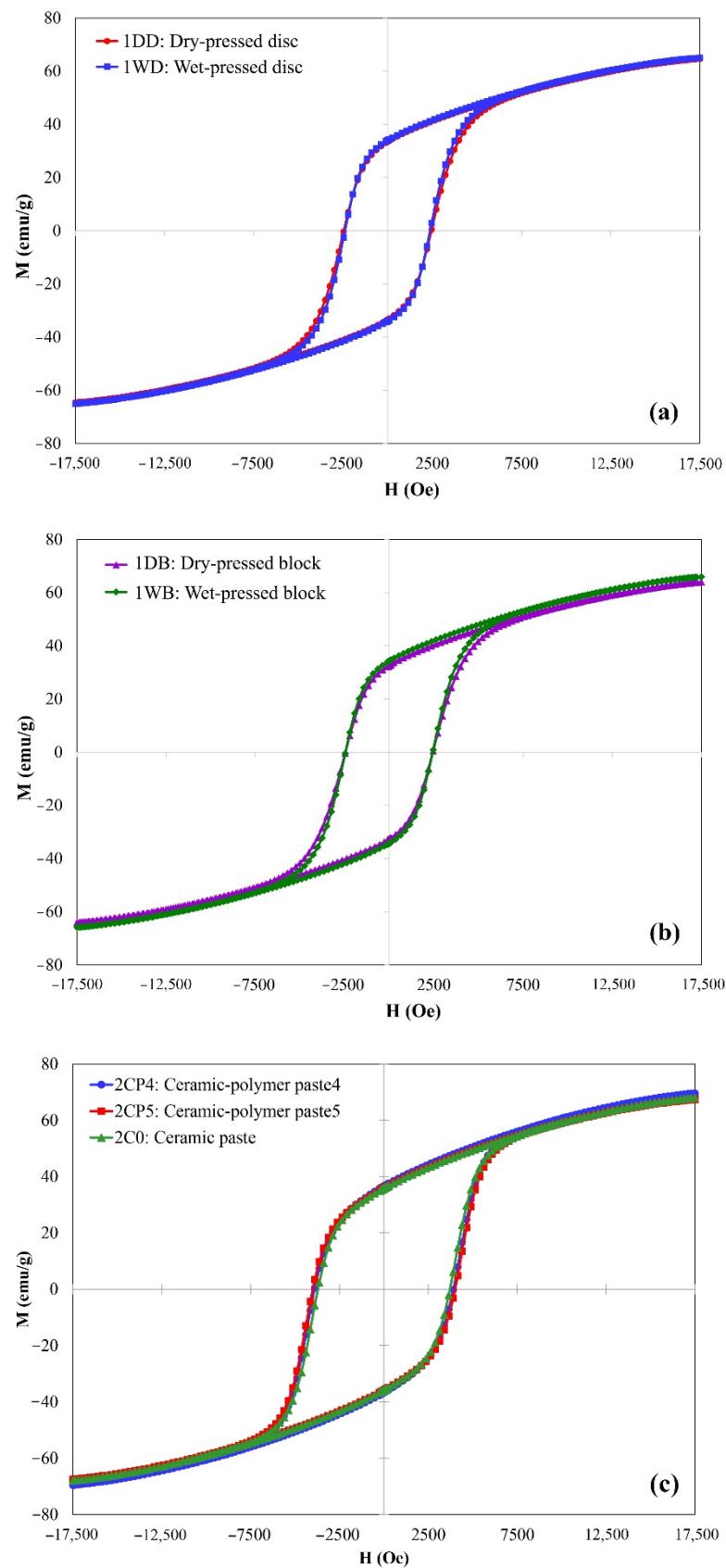


**Figure 5.** Hysteresis loops of (a) dry- and wet-pressed disc magnets; (b) dry- and wet-pressed bar magnets; (c) magnets from paste-injection molding.

#### 4. Conclusions

The densities and magnetic properties of isotropic BaFe<sub>12</sub>O<sub>19</sub> magnets sintered at 1150 °C for 5 h depended on the fabrication methods. However, the dry-pressed magnets from sol-gel-derived powders were not influenced by their shapes. When adding DI water in the compaction, the increase in magnetization and decrease in coercivity was modest. Facile paste-injection molding produced BaFe<sub>12</sub>O<sub>19</sub> magnets with reproducible density and magnetic properties. The 1.90–2.35 g/cm<sup>3</sup> magnets obtained from ceramic-polymer pastes have larger coercivities than those of the higher-density compact magnets. By using a ceramic paste without polymer additives, a slightly higher magnetization was obtained at the expense of enhanced coercivity. The magnetization is related to the phase purity and uniformity in elemental composition of BaFe<sub>12</sub>O<sub>19</sub>. On the other hand, the variation in coercivity is majorly influenced by the particle size distribution.

**Author Contributions:** Conceptualization, C.S. and T.C.; methodology, W.T. and T.C.; formal analysis, W.T. and P.J.; data curation, W.T. and P.J.; writing—original draft preparation, C.S. and T.C.; writing—review and editing, C.S.; project administration, C.S.; funding acquisition, C.S. All authors have read and agreed to the published version of the manuscript.

**Funding:** This work is funded by Thailand Center of Excellence in Physics (ThEP-63-PIP-WU3).

**Institutional Review Board Statement:** Not applicable.

**Informed Consent Statement:** Not applicable.

**Data Availability Statement:** The data presented in this study are available on request from the corresponding author.

**Acknowledgments:** The authors acknowledge facility support from Chesta Ruttanapun of King Mongkut's Institute of Technology Ladkrabang, and Komkrich Chokprasombat of Thaksin University. XRD and SEM are characterized at Nanotechnology and Materials Analytical Instrument Service Unit (NMIS) of College of Materials Innovation and Technology, and Scientific Instruments Center of School of Science, King Mongkut's Institute of Technology Ladkrabang, respectively.

**Conflicts of Interest:** The authors declare no conflict of interest.

#### References

1. Pullar, R. Hexagonal ferrites: A review of the synthesis, properties and applications of hexaferrite ceramics. *Prog. Mater. Sci.* **2012**, *57*, 1191–1334. [[CrossRef](#)]
2. de Julián Fernández, C.; Sangregorio, C.; de la Figuera, J.; Belec, B.; Makovec, D.; Quesada, A. Progress and prospects of hard hexaferrites for permanent magnet applications. *J. Phys. D Appl. Phys.* **2021**, *54*, 153001. [[CrossRef](#)]
3. Frenea-Robin, M.; Marchalot, J. Basic principles and recent advances in magnetic cell separation. *Magnetochemistry* **2022**, *8*, 11. [[CrossRef](#)]
4. Granados-Miralles, C.; Jenuš, P. On the potential of hard ferrite ceramics for permanent magnet technology: A review on sintering strategies. *J. Phys. D Appl. Phys.* **2021**, *54*, 303001. [[CrossRef](#)]
5. Brightlin, B.C.; Balamurugan, S. The effect of post annealing treatment on the citrate sol-gel derived nanocrystalline BaFe<sub>12</sub>O<sub>19</sub> powder: Structural, morphological, optical and magnetic properties. *Appl. Nanosci.* **2016**, *6*, 1199–1210. [[CrossRef](#)]
6. Faisal, M.; Saeed, A.; Larik, F.A.; Ghumro, S.A.; Rasheed, S.; Channar, P.A. Wows sol-gel based synthesis and structural, morphological, electrical and magnetic characterization of Co-Sm doped M-type barium hexaferrite materials. *J. Electron. Mater.* **2018**, *47*, 7011–7022. [[CrossRef](#)]
7. Asghar, G.; Asri, S.; Khusro, S.N.; Tariq, G.H.; Awan, M.S.; Irshad, M.; Safeen, A.; Iqbal, Y.; Shah, W.H.; Anis-Ur-Rehman, M. Enhanced magnetic properties of barium hexaferrite. *J. Electron. Mater.* **2020**, *49*, 4318–4323. [[CrossRef](#)]
8. Charoensuk, T.; Thongsamrit, W.; Ruttanapun, C.; Jantaratana, P.; Sirisathitkul, C. Loading effect of sol-gel derived barium hexaferrite on magnetic polymer composites. *Nanomaterials* **2021**, *11*, 558. [[CrossRef](#)] [[PubMed](#)]
9. Kristiantoro; Idayanti; Dedi; Sudrajat; Mulyadi; Gustinova. Influence of compaction pressure on magnetic characteristics, density, and hardness of barium hexaferrite. *IOP Conf. Ser. Mater. Sci. Eng.* **2019**, *620*, 012106. [[CrossRef](#)]
10. Timofeev, A.V.; Kostishin, V.G.; Makeev, D.B.; Chitanov, D.N. Magnetic properties of barium hexaferrite compacted nanopowders. *Tech. Phys.* **2019**, *64*, 1484–1487. [[CrossRef](#)]
11. Vinnik, D.A.; Chernukha, A.S.; Gudkova, S.A.; Zhivulin, V.E.; Trofimov, E.A.; Tarasova, A.Y.; Zherebtsov, D.A.; Kalandija, M.; Trukhanov, A.V.; Trukhanov, S.V.; et al. Morphology and magnetic properties of pressed barium hexaferrite BaFe<sub>12</sub>O<sub>19</sub> materials. *J. Magn. Magn. Mater.* **2018**, *459*, 131–135. [[CrossRef](#)]

12. Chaudhary, V.; Mantri, S.A.; Ramanujan, R.V.; Banerjee, R. Additive manufacturing of magnetic materials. *Prog. Mater. Sci.* **2020**, *114*, 100688. [[CrossRef](#)]
13. Wei, X.; Liu, Y.; Zhao, D.; Mao, X.; Jiang, W.; Ge, S.S. Net-shaped barium and strontium ferrites by 3D printing with enhanced magnetic performance from milled powders. *J. Magn. Magn. Mater.* **2020**, *493*, 165664. [[CrossRef](#)]
14. Anjum, S.; Sehar, F.; Mustafa, Z.; Awan, M.S. Enhancement of structural and magnetic properties of M-type hexaferrite permanent magnet based on synthesis temperature. *Appl. Phys. A* **2018**, *124*, 49. [[CrossRef](#)]
15. Azis, R.A.S.; Che Muda, N.N.; Hassan, J.; Shaari, A.H.; Ibrahim, I.R.; Mustafa, M.S.; Sulaiman, S.; Matori, K.A.; Fen, Y.W. Effect of ratio in ammonium nitrate on the structural, microstructural, magnetic, and AC conductivity properties of BaFe<sub>12</sub>O<sub>19</sub>. *Materials* **2018**, *11*, 2190. [[CrossRef](#)] [[PubMed](#)]
16. Shalini, M.G.; Subha, A.; Sahu, B.; Sahoo, S.C. Phase evolution and temperature dependent magnetic properties of nanocrystalline barium hexaferrite. *J. Mater. Sci. Mater. Electron.* **2019**, *30*, 13647–13654. [[CrossRef](#)]
17. Lohmaah, A.; Chokprasombat, K.; Pinitsoontorn, S.; Sirisathitkul, C. Magnetic properties and morphology copper-substituted barium hexaferrites from sol-gel auto-combustion synthesis. *Materials* **2021**, *14*, 5873. [[CrossRef](#)] [[PubMed](#)]